Parametric Identification of Stochastic Dynamic Model of Human Visuomotor Tracking Control

Shigeki Matsumoto and Katsutoshi Yoshida

***Abstract*— We conducted an experiment on a visuomotor tracking task using human participants and compared it with numerical simulations on a stochastic dynamic model of the same task. Our numerical model comprises additive and multiplicative white Gaussian noises and a state feedback term. The parameters of the numerical model were identified using particle swarm optimization. To examine the stochastic behavior of the tracking task, we experimentally estimated the probability density functions (PDFs) of the state variables. Three of the four experimentally obtained PDFs show good agreement with those numerically obtained by the proposed model.**

I. INTRODUCTION

Human balancing tasks such as maintaining an upright posture and balancing a stick on the fingertip have been studied using various approaches, notably those based on stabilization control of an inverted pendulum [1–2]. In a similar way, a visuomotor tracking task is studied as one of the human balancing tasks on visual feedback [3]. This paper studies such a visuomotor tracking task.

In general, human movements display random fluctuations, leading some researchers [1–8] to adopt a statistical approach to human balancing and tracking control using probability density function (PDF). For example, Cabrera et al. [4] and Suzuki et al. [5] confirmed that the PDF of the change in speed of the fingertip during stick balancing by skilled subjects had broader tail than that by unskilled subjects. Cabrera [4] argued that changes in speed of hand movements during stick balancing were best described by a truncated Lèvy distribution (a type of fat-tailed distribution). In other studies adopting PDFs, Nomura et al. [6–7] and Gawthrop et al. [8] confirmed that bimodal stabilization distributions were observed in experiments on quiet standing. They replicated similar bimodal distributions using their control models.

In early studies [4,6–7], the numerical models of the human movements are constructed to reproduce the PDFs qualitatively. However, the quantitative reproduction of the PDFs is required to design human-like artificial motion.

In this study, we investigate a simulated tracking control model that reproduces the PDFs of the human visuomotor tracking task quantitatively and accurately. Our control model comprises additive and multiplicative white Gaussian noises and a state feedback term. The parameters of the control model are then identified using particle swarm optimization (PSO) to minimize the squared residuals between the PDFs of the human participant and those of a control model.

S. Matsumoto and K. Yoshida are with the Department of Mechanical and Intelligent Engineering Utsunomiya University Yoto 7-1-2, Utsunomiya, Tochigi 321-8585, Japan matsumoto@katzlab.jp

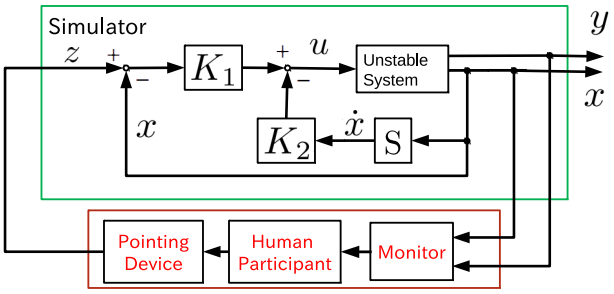

Fig. 1. Experimental system.

The experiment is conducted using a virtual tracking system [9]. The common virtual mechanical system (controlled system) links the experiment and the control model. This approach is inspired by previous studies [3,5,8].

II. EXPERIMENTAL SYSTEM

A. Virtual Mechanical System

The experimental system is shown in Fig. 1. The system comprises a numerical simulator of an unstable mechanical system, a pointing device, and a monitor. The monitor displays the motions of the mechanical system. Participants track the motion of a target on the monitor and manipulated the pointing device in order to stabilize the system using a cursor. The target is repelled by the cursor.

The animation window in Fig. 2 shows the tracking target and hand cursor, represented by the thick and thin lines, respectively. The distance between the lines represents the tracking error.

The monitor resolution is 1200×600 (pixels), and the range of the displacement $(-3, 3)$ in the numerical model is mapped to the horizontal range of pixels $(1, 1200)$ in the window.

Cursor manipulation is achieved using a tracking control that allows the cursor to track a target orbit z. The target orbit z is measured from the pointing device and fed into the numerical simulator with a sampling period Δt, while the tracking image on the monitor is animated at the same rate.

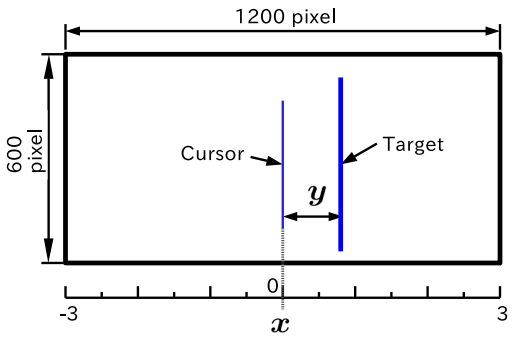

Fig. 2. Design of the animation window.

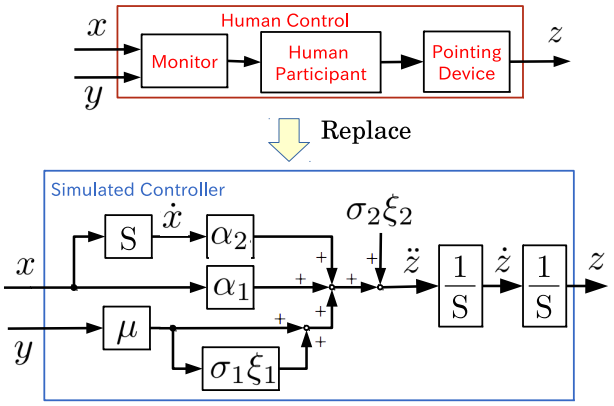

Fig. 3. Tracking control module.

B. Equations of Motion

The equations of motion of the unstable system in Fig. 1 are given by

$$\ddot{x} = -\gamma\dot{x} - \alpha y + u, \tag{1a}$$

$$\ddot{y} = -\gamma\dot{y} + 2\alpha y - u, \tag{1b}$$

where α is a stiffness coefficient, γ is a viscous damping coefficient, x is an absolute position of the cursor, y is a tracking error, and u is an external force. We set the system parameters of (1) at $\alpha = 22$ and $\gamma = 6$, the same values as those used in our previous study [9].

The state vector of (1), can be defined by

$$\boldsymbol{x} = (x_1, x_2, x_3, x_4)^T := (x, \dot{x}, y, \dot{y})^T. \tag{2}$$

C. Tracking Control System

We assumed the target orbit $z(t)$ as a given time function. The tracking control input u that allows the cursor position x to track the target orbit $z(t)$ is defined as follows:

$$u = -K_1(z(t) - x) - K_2\dot{x}, \tag{3}$$

where K_1 and K_2 are the gains of the cursor position and velocity, respectively. We set $K_1 = 5000$, $K_2 = 200$, and the initial state vector $\boldsymbol{x}(0) = (0, 0, 0.1, 0)^T$.

For numerical integration of (1) and (3), a fourth-order Runge–Kutta–Gill method was employed with a time step of 1×10^{-3} s.

III. EXPERIMENT ON THE TRACKING TASK

A. Experimental Data

In the experimental system shown in Fig. 1, we measured the state vector of the human tracking task as $\boldsymbol{x}(t_i; s, n)$, $0 \leqq t_i \leqq t_I$, where t_i is a discrete time with a sampling period Δt, s is an index of participants, n is an index of trials, and I is the length of the time series

B. Estimation Method

We define a population $\boldsymbol{\Pi}$ of trials as

$$\boldsymbol{\Pi} := \{(s, n) | \quad 1 \leqq s \leqq S, \quad 1 \leqq n \leqq N\}, \tag{4}$$

where S is the number of participants and N is the number of trials for each participant. We then construct a PDF of the state variable x_k obtained from the nth trial of the sth participant as $P_H^{(s,n)}(x_k)$ and derived an average of $P_H^{(s,n)}(x_k)$ for population $\boldsymbol{\Pi}$ as

$$P_H(x_k) = \frac{1}{SN}\sum_{s=1}^{S}\sum_{n=1}^{N} P_H^{(s,n)}(x_k). \tag{5}$$

For numerical construction of $P_H^{(s,n)}(x_k)$, we set the number of the histogram bins to $n_\phi = 300$ and the bin width $\Delta\phi_k$ as,

$$\Delta\phi_k = \frac{1}{n_\phi}(\phi_k^u - \phi_k^l), \tag{6}$$

where ϕ_k^u and ϕ_k^l are the upper and lower limits of x_k, respectively. In this study, we set these limits to $(\phi_1^l, \phi_1^u) = (\phi_2^l, \phi_2^u) = (\phi_4^l, \phi_4^u) = (-3, 3)$, $(\phi_3^l, \phi_3^u) = (-1, 1)$.

C. Experimental Procedure

Participants were healthy males in their early 20s. They were first instructed on the operation of the experimental system, the number of trials, and the duration of each trial. In each trial, the participant watched the motion of the target and manipulated the pointing device so that the cursor tracked the target. Several practice trials were performed prior to measurement. An audio signal began the trial, and the participant attempted to maintain the tracking until time t_I. The trial was repeated if the target or the cursor exceeded the limits of the window for $t < t_I$.

As the number of participants was $S = 4$ and the number of trials for each participant was $N = 20$, the number of samples (elements of set $\boldsymbol{\Pi}$) was $S \times N = 80$. The sampling period was $\Delta t = 0.02$ s and the length of the time series was $I = 16384$ with the time interval of 340 s.

IV. SIMULATED TRACKING CONTROL MODEL

Human control was then replaced by a simulated tracking control model with inputs x and y and output z, as shown in Fig. 3. The simulator (surrounded by the green frame in Fig. 1) replicated the human experiment using the identical numerical simulator.

A. Target Orbit Equivalent to State Feedback Control

By the selected gains $K_1 = 5000$ and $K_2 = 200$ in (3), we obtain $x \approx z(t)$. Thus, assuming the forced displacement $x = z(t)$, we have

$$u = \ddot{x} + \gamma\dot{x} + \alpha y = \ddot{z}(t) + \gamma\dot{z}(t) + \alpha y. \tag{7}$$

On the other hand, a state feedback controller of the cursor position x and tracking error y is introduced:

$$u := F_1 x + F_2\dot{x} + F_3 y + F_4\dot{y}. \tag{8}$$

Equating (7) and (8) by u gives

$$\ddot{z}(t) + \gamma\dot{z} + \alpha y = u = F_1 x + F_2\dot{x} + F_3 y + F_4\dot{y}. \tag{9}$$

Therefore, we have obtained

$$\ddot{z}(t) + \gamma\dot{z} = F_1 x + F_2\dot{x} + (F_3 - \alpha)y + F_4\dot{y}. \tag{10}$$

For simplicity, we assume $F_4 = 0$ and $\dot{z}(t) = \dot{x}$ in (10) to obtain

$$\ddot{z}(t) = F_1 x + (F_2 - \gamma)\dot{x} + (F_3 - \alpha)y. \tag{11}$$

This differential equation provides a dynamic model of the target orbit $z(t)$.

B. Introducing Fluctuations

We treat the proportional gain of the tracking error $(F_3 - \alpha)$ in (11) as a white Gaussian noise with mean μ and variance σ_1^2, following the control models in Ushida et al. [1] and Cabrera et al. [2].

We also introduce an additive noise to overcome the problem discussed by Nakao [10] wherein the stochastic variable converges to zero in the system having the multiplicative noise only. The additive noise is a white Gaussian noise with zero mean and variance σ_2^2. This results in

$$\ddot{z}(t) = F_1 x + (F_2 - \gamma)\dot{x} + \mu(1 + \sigma_1\xi_1)y + \sigma_2\xi_2 \tag{12}$$

$$=: \alpha_1 x + \alpha_2\dot{x} + \mu(1 + \sigma_1\xi_1)y + \sigma_2\xi_2. \tag{13}$$

This differential equation provides the control model. Its block diagram is shown in Fig. 3. The unknown parameters of the control model (13) are

$$\boldsymbol{p} = (p_1, \ldots, p_5) := (\alpha_1, \alpha_2, \mu, \sigma_1, \sigma_2). \tag{14}$$

C. PDF of the Control Model

We define a sample path of the control model (13) with parameters $\boldsymbol{p}$ as $x_k(t_i, n'; \boldsymbol{p})$, where n' is an index of the sample path of the control model. In practice, we obtained the individual sample paths by changing the seed of the pseudo random number generator. We then construct the PDF with respect to x_k on the basis of a sample path $x_k(t_i, n'; \boldsymbol{p})$ as $P_A^{n'}(x_k; \boldsymbol{p})$. We take an average of $P_A^{n'}(x_k; \boldsymbol{p})$ as

$$P_A(x_k; \boldsymbol{p}) = \frac{1}{N'} \sum_{n'=1}^{N'} P_A^{n'}(x_k; \boldsymbol{p}), \tag{15}$$

where $N' = 80$ is the number of sample paths. This PDF represents fluctuations arising in the control model. For numerical construction of $P_A(x_k; \boldsymbol{p})$, we set limits of (ϕ_k^l, ϕ_k^u) and the histogram bins n_ϕ to those used in the human experiment.

V. METHOD OF PARAMETER IDENTIFICATION

A. Parameter Identification

To estimate the parameters $\boldsymbol{p}$ such that $P_A(x_k; \boldsymbol{p})$ becomes $P_A(x_k; \boldsymbol{p}) \approx P_H(x_k)$, we solve the following optimization problem:

$$\begin{cases} \underset{\boldsymbol{p}}{\text{Minimize}}\, E(\boldsymbol{p}), \\ E(\boldsymbol{p}) := \sum_{k=1}^{4} a_k E_k(\boldsymbol{p}), \\ E_k(\boldsymbol{p}) = \int_{\phi_k^l}^{\phi_k^u} \{P_H(x_k) - P_A(x_k; \boldsymbol{p})\}^2 dx_k, \end{cases} \tag{16}$$

where a_k represents a weight coefficient for the state variable x_k and ϕ_k^u and ϕ_k^l represent the upper and lower limits of x_k, respectively. In this study, we set $a_1 = a_2 = a_3 = a_4 = 1$.

B. Particle Swarm Optimization

We employ PSO to solve (16). PSO is a population-based optimization tool used to solve function optimization problems or problems that can be transformed into function optimization problems. It mimics the swarming behavior observed in flocks of birds, schools of fish, swarms of bees, and some aspects of human social behavior. We use a standard algorithm, following [11].

Consider an optimization problem of the following form:

$$\underset{\boldsymbol{p}}{\text{Minimize}}\, E(\boldsymbol{p}), \tag{17}$$

where $\boldsymbol{p} := (p_1, \ldots, p_j, \ldots, p_M) \in \mathbb{D} \subset \mathbb{R}^M$ is an M-dimensional vector and the cost $E(\boldsymbol{p})$ is assumed to be a positive definite real-valued function. In PSO, a swarm is composed of N_p candidate solutions $\{\boldsymbol{p}^1, \ldots, \boldsymbol{p}^i, \ldots, \boldsymbol{p}^{N_p}\}$ called particles. The particles explore the M-dimensional domain $\mathbb{D}$ in search of the global solution $\boldsymbol{p}_0$ given by

$$\boldsymbol{p}_0 = \arg\min_{\boldsymbol{p}} E(\boldsymbol{p}). \tag{18}$$

The positions of the particles are recursively updated by

$$\begin{cases} \boldsymbol{p}^i(l+1) = \boldsymbol{p}^i(l) + \boldsymbol{v}^i(l), \\ \boldsymbol{v}^i(l+1) = \rho_0(l)\boldsymbol{v}^i(l) + \rho_1(l)\{\boldsymbol{P}^i(l) - \boldsymbol{p}^i(l)\} \\ \qquad\qquad +\rho_2(l)\{\boldsymbol{G}(l) - \boldsymbol{p}^i(l)\}, \end{cases} \tag{19}$$

where $\boldsymbol{p}^i(l)$ is the position of the ith particle at iteration l, $\boldsymbol{v}^i(l)$ is the corresponding velocity, and $\rho_0(l)$, $\rho_1(l)$, and $\rho_2(l)$ are random numbers. $\boldsymbol{P}^i(l)$ is called the personal best: the ith particle position taking the lowest cost among $\boldsymbol{p}^i(0), \ldots, \boldsymbol{p}^i(l)$. $\boldsymbol{G}(l)$ is called the global best: the particle position that has the lowest cost among all the particles for all iterations. Therefore, the optimization solution $\boldsymbol{p}_0$ in (16) is approximated by

$$\boldsymbol{p}_0 \approx \boldsymbol{G}(l). \tag{20}$$

In this study, $\rho_0(l)$, $\rho_1(l)$, and $\rho_2(l)$ are taken as uniform random numbers over the intervals $[0.6, 1.2]$, $[0, 0.12]$, and $[0, 0.06]$, respectively.

The initial search domain $\mathbb{D}_0 \subset \mathbb{D}$ is taken as an M-dimensional hypercuboid:

$$\mathbb{D}_0 := [b_1, c_1] \times \ldots \times [b_M, c_M], \tag{21}$$

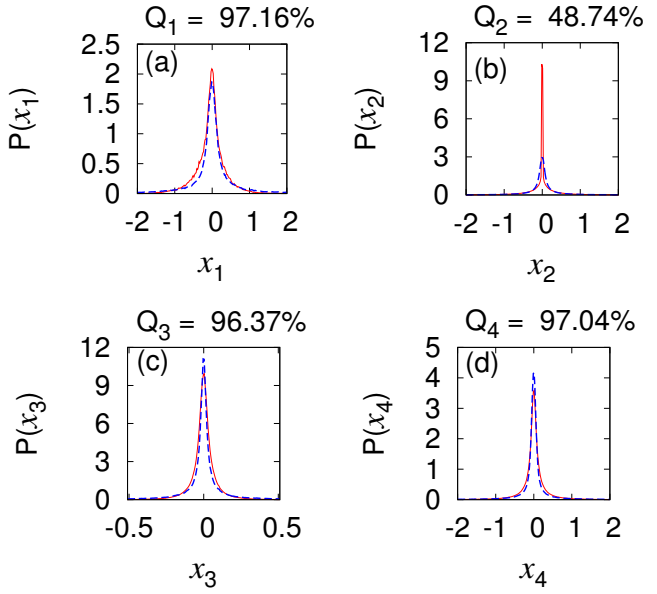

Fig. 4. PDFs of the human participants and control model. Solid lines in red and broken lines in blue represent manipulation by the human participants and control model, respectively. (a) x_1, (b) x_2, (c) x_3, and (d) x_4.

where b_j and c_j are the minimum and maximum points of the initial parameters, respectively.

The initial particle positions $\boldsymbol{p}^i(0)$ are taken N_p uniform grid points on $\mathbb{D}_0$, where $N_p = n_1 \times \ldots \times n_5$. Thus, N_p represents the number of the particles. All the initial particle velocities are set to zero.

C. Identification Condition

The condition of identification is empirically selected as follows. We set the PSO parameter to $M = 5$, $n_1 = n_5 = 2$ and $n_2 = n_3 = n_4 = 3$; hence, the number of particles is $N_p = 2^2 \times 3^3 = 108$. The initial search domain in (21) is taken as

$$\mathbb{D}_0 = [0, 3] \times [-10, 3] \times [25, 50] \times [0, 6] \times [0, 6]. \quad (22)$$

The number of iterations l is 400.

VI. IDENTIFICATION RESULTS FOR THE CONTROL MODEL

A. Main Result

Table I shows the identified model parameters $\boldsymbol{p}_0$, defined in the control model (13). The cost for the parameters $\boldsymbol{p}_0$ is obtained as $E(\boldsymbol{p}_0) = 2.57$.

TABLE I: IDENTIFIED MODEL PARAMETERS.

Components	Values
α_1	1.64
α_2	-10.32
μ	40.35
σ_1	2.57
σ_2	1.68

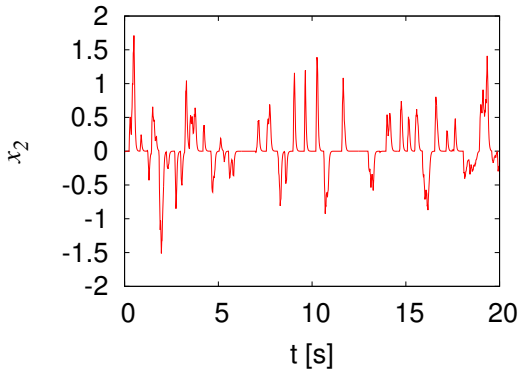

Fig. 5. Cursor velocity x_2 of a human participant.

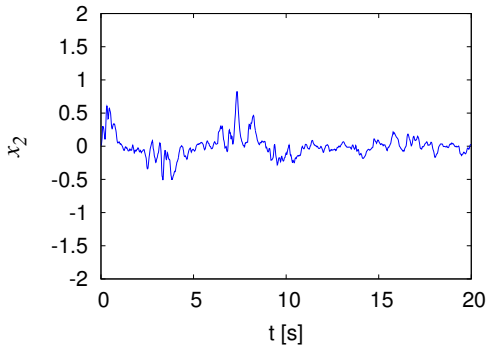

Fig. 6. Cursor velocity x_2 of the identified control model.

Fig. 4 shows a comparison of the identified control model and the human tracking control. Solid lines in red and broken lines in blue represent the PDFs of the human participants: $P_H(x_k)$, and the control model: $P_A(x_k; \boldsymbol{p})$, respectively. Fig. 4 shows the results for (a) cursor position x_1, (b) cursor velocity x_2, (c) tracking error x_3, and (d) time derivative of tracking error x_4.

A numerical measure of goodness of fit is introduced for the model quality Q_k, as

$$\begin{cases} Q_k := (1 - \frac{E_k}{O_k}) \times 100\%, \\ O_k := \int_{\phi_k^l}^{\phi_k^u} \{P_H(x_k)\}^2 dx_k, \end{cases} \quad (23)$$

where E_k is the cost for each state variable x_k as defined in (16).

In Fig. 4 (a), (c), and (d), the simulated PDFs $P_A(x_k; \boldsymbol{p})$ are in good agreement with the human PDFs $P_H(x_k)$ for $k = 1, 3, 4$, at $Q_1 = 97.16\%$ $Q_3 = 96.37\%$ and $Q_4 = 97.04\%$, respectively. However, as shown in Fig. 4 (b), the PDF $P_A(x_2; \boldsymbol{p})$ is not in good agreement with $P_H(x_2)$ at around $x_2 = 0$; the model quality $Q_2 = 48.74\%$ is low.

In our preliminary experiments on individual participants, we obtained model qualities comparable to the above results without changing the structure of the control model (13). This means that the mathematical structure of the control model (13) has robustness against the change of participants.

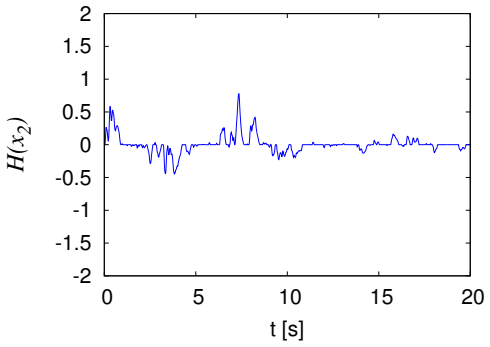

Fig. 7. Time series of $H(x_2)$.

B. Consideration on Results

We analyze the time series to investigate why the model quality Q_2 of cursor velocity x_2 is low. The time series of cursor velocity $x_2(t)$ for the human participants and control model are shown in Fig. 5 and Fig. 6, respectively. In the case of the human participants, time series $x_2(t)$ sometimes stops at $x_2 = 0$ (Fig. 5). On the other hand, in the case of the control model, time series $x_2(t)$ usually does not stop at $x_2 = 0$ (Fig. 6).

One explanation for the stopping at $x_2 = 0$ seems to be given as existence of a deadband characteristic. For example, we consider x_2 transformed by a deadband function as

$$H(x_2) = \begin{cases} \beta_1(x_2 + \beta_2) & if(x_2 \leqq -\beta_2), \\ \beta_1(x_2 - \beta_2) & if(x_2 \geqq \beta_2), \\ 0 & otherwise. \end{cases} \quad (24)$$

Fig. 7 shows an example of time series $H(x_2)$, where the parameters in (24) are $\beta_1 = 1$ and $\beta_2 = 0.05$. The time series in Fig. 7 intermittently stops at $H(x_2) = 0$, similar to the time series of the human participant in Fig. 5. The low model quality Q_2 at cursor velocity x_2 can therefore be explained by the absence of deadband characteristics in the control model.

We may propose two hypotheses regarding the deadband characteristics of the human participants. The first hypothesis concerns Coulomb friction in the pointing device. When human participants stop the device, a constant force is required to move it again. The second hypothesis concerns the function of the human nervous system. It is possible that human participants are unable to react to the dynamics of the mechanical model when the tracking error y is sufficiently small.

VII. CONCLUSION

In this study, we have proposed a simulated tracking control model that quantitatively and accurately reproduced the PDFs of human tracking. We developed a control model comprising an additive noise, a multiplicative noise, and a state feedback term. We identified the parameters of the control model using a PSO that minimized the squared residuals between the PDFs of the human participant and control model.

The results of PDFs for the cursor position x_1, the tracking error x_3, and the time derivative of the tracking error x_4, showed good agreement between the experiment and the control model, with model qualities $Q_1 = 97.16\%$ $Q_3 = 96.37\%$ and $Q_4 = 97.04\%$. However, the model quality for cursor velocity x_2 was low at $Q_2 = 48.74\%$.

In future, we plan to introduce the deadband characteristics to the control model in order to improve the model quality of cursor velocity x_2. We also plan to test the hypotheses stated in Section VI-B.

REFERENCES

[1] Ushida, S., Fukuda, K., LEE, J., and Deguchi, K., Bio-Mimetic Control of Inverted Pendulum Systems with Time-Delay, *Transactions of the Institute of Systems Control and Information Engineers*, Vol. 20, No. 4, pp. 160-166, 2007 (in Japanese).

[2] Cabrera, J. L., and Milton, J. G., On-Off Intermittency in a Human Balancing Task, *Physical Review Letters*, Vol. 89, No. 15, pp. 158702:1-4, 2002.

[3] Bormann, R., Cabrera, J. L., Milton, J. G., and Eurich, C. W., Visuomotor Tracking on a Computer Screen- An Experimental Paradigm to Study the Dynamics of Motor Control, *Neurocomputing*, Vol. 58, No. 60, pp. 517-523, 2004.

[4] Cabrera, J. L., and Milton, J. G., Human Stick Balancing: Tuning Lèvy Flights to Improve Balance Control, *CHAOS*, Vol. 14, No. 3, pp. 691-698, 2004.

[5] Suzuki, S., Harashima, F., and Furuta, K. Human Control Law and Brain Activity of Voluntary Motion by Utilizing a Balancing Task with an Inverted Pendulum, *Advances in Human-Computer Interaction*, Vol. 2010, pp. 215825:1-16, 2010.

[6] Bottaro, A., Yasutake, Y., Nomura, T., Casadio, M., and Morasso, P., Bounded Stability of the Quiet Standing Posture: An Intermittent Control Model, *Human Movement Science*, Vol. 27, pp. 473495, 2008.

[7] Taniguchi, S., and Nomura, T., An Anticipatory and Low-gain Neural-feedback Control Strategy Acquired during Motor Learning of a Balance Task, *IEICE Technical Report NC*, Vol. 105, No. 659, pp. 37-42, 2006 (in Japanese).

[8] Gawthrop, P., Loram, I., Lakie, M., and Gollee, H., Intermittent Control: A Computational Theory of Human Control, *Biological Cybernetics*, Vol. 104, No. 1-2, pp. 104:31-51, 2011.

[9] Matsumoto, S., Yoshida, K., and Higeta, A., An Experimental Study on Coupled Balancing Tasks between Human Subjects and Artificial Controllers, *Transactions of the Institute of Systems Control and Information Engineers*, Vol. 26, No. 11, pp. 407-414, 2013.

[10] Nakao, H., Asymptotic Power Law of Moments in a Random Multiplicative Process with Weak Additive Noise, *Physical Review E*, Vol. 58, No. 2, pp. 1591-1600, 1998.

[11] Saito, T., Particle Swarm Optimizers and Nonlinear Systems, *IEICE Fundamentals Review*, Vol. 5, No. 2, pp. 155-161, 2011 (in Japanese).